Strange Particle Production in p-p collisions at ALICE

Rabia Aslam
Supervisors: Jean-Pierre Revol and Adam Jacholkowski
CERN Summer Student 2011

November 17, 2011

Abstract

In this project, the production of strange particles is studied in proton-proton collisions at center of mass energy, $\sqrt{s} = 7$ TeV at ALICE detector in LHC. K^0_s mesons and Λ baryons are constructed from their decay topologies. Some basic kinematic properties like invariant mass distribution and decay length of K^0_s is plotted and its life time is calculated. Multiplicity Dependence of K^0_s is also determined. The results are produced for both real and monte-carlo simulated data for comparison. The project involves use of ROOT and AliROOT for the analysis of both types of data sets.

1 Introduction

1.1 LHC at CERN

The Large Hadron Collider (LHC) built at CERN (European Organization for Nuclear Research) is the world's largest and highest-energy particle accelerator. The LHC tunnel (27 km in circumference and as deep as 175 meters) collides opposing particle beams of protons at center-of-mass energy $\sqrt{s} = 7$ TeV and $\sqrt{s} = 2.76$ TeV per nucleon pair in lead-lead collisions. The information gathered as a result of these collisions is expected to answer some big and most fundamental questions of physics concerning deepest laws of physics governing the interactions and forces among the elementary objects. It will also help in understanding completely the structure of space and time and intersection of quantum mechanics and general relativity where current theories and knowledge is unclear or breakdowns altogether. Higgs mechanism for generating elementary particle masses is the excited phenomenon which LHC is expected to explain. These high energy particle collisions will also throw some light on extra dimensions, super-symmetry, nature of the dark matter, questions about early universe and the big bang. Scientists from all around the globe are hopeful that the LHC ring will unveil the facts about the

most serious questions of Physics today.

LHC has six detectors, all of which are located underground. These are ATLAS (A Toroidal LHC apparatus), CMS (Compact Muon Solenoid), ALICE (A Large Ion Collider Experiment), LHCb (Large Hadron Collider beauty), TOTEM (Total Elastic and diffractive cross section Measurement) and LHCf (Large Hadron Collider forward) as shown in figure 1.

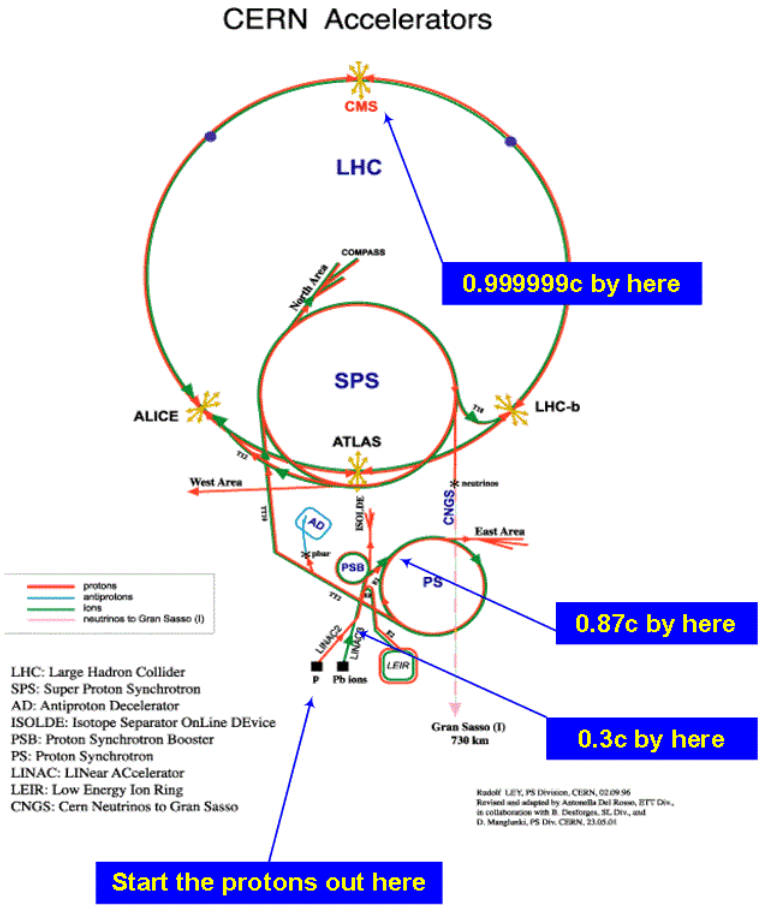

Figure 1: Large Hadron Collider (LHC) at CERN

1.2 ALICE experiment at CERN

ALICE experiment was designed to study the physics of strongly interacting matter and the quark-gluon plasma believed to have existed in early universe. Besides running with lead ions (heavy ions), it also includes elementary proton-proton collisions. It consists of a central detector system covering mid-rapidity over the full azimuth installed inside a large solenoidal magnet which generates a magnetic field of ≤ 0.5 T and several forward systems [1]. The central barrel includes:

- an Inner Tracking System (ITS) that consists of six cylindrical layers of Silicon detectors, this system is optimized for the reconstruction of secondary

vertices from the decays of heavy quarks and for precise tracking and identification of low-p_T particles

- a Time Projection Chamber (TPC) which is the main device in ALICE central barrel for tracking of charged particles and particle identification,
- a Transition Radiation Detector (TRD) which provides electron identification with momenta greater than 1 GeV/c
- and an array of detectors (TOF) for particle identification in the momentum region from 0.2 to 2.5 GeV/cg [2]

The various parts of the detector are shown in figure 2.

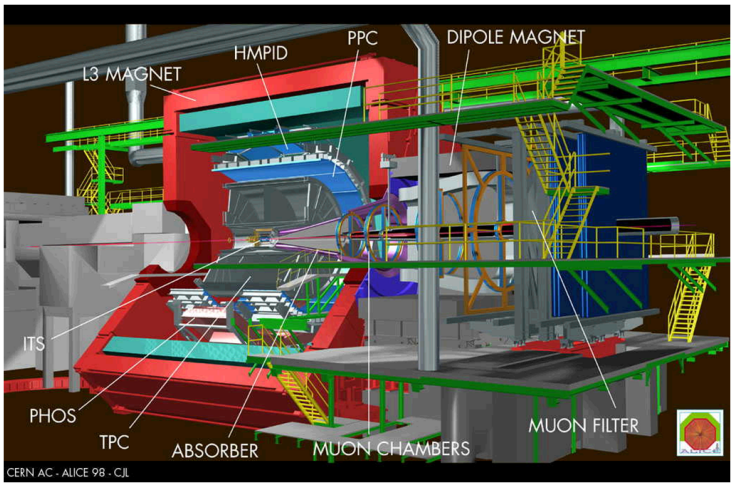

Figure 2: ALICE detector

1.3 Proton-Proton collisions in ALICE

Measurements of proton-proton (pp) collisions are an important part of the ALICE program as a reference for the results obtained in heavy ions collisions. Several features of ALICE provide unique information about low-momentum region in pp collisions at the LHC where most particles are produced and which therefore contributes most to the underlying event.

For pp collisions the goal is to be able to read out the experiment at rates of at least 1.4 kHz. Since the specific features of the used detectors (TPC drift time of almost 100 μs) makes it a rather slow detector (at least compared to the three other large LHC experiments), the luminosity for pp collisions has to be limited at $\sim 5 \times 10^{30} cm^{-2} s^{-1}$, corresponding to an interaction rate of $\sim$ 200 kHz, the integrated luminosity can be maximized for rare processes. With lower luminosity (10^{29} $cm^{-2} s^{-1}$) statistics for large cross section observables can be collected and global event properties can be studied at optimum detector performance.

1.4 Standard Model

The Standard Model (SM) is nowadays the accepted theory for describing elementary particles and their fundamental interactions. According to the SM, there are only two types of particles making everything around us, constituents of matter and interaction's carriers.
Constituents of matter particles are fermions, and are divided in two groups, the quark's group (there are 6 quark flavors, *up*, *down*, *charm*, *strange*, *top* and *bottom*), and the lepton's group (*electron*, *muon*, *tau*, and their corresponding neutrinos). While leptons exist as free particles, quarks appear in normal nuclear matter only as confined quantum states called hadrons.

There are 4 fundamental interactions: strong, electromagnetic, weak, and gravitational interactions. According to the SM, interactions between particles are due the exchange of an intermediate messenger called exchange particle that is a boson. The strength of the interaction is related with the mass of this particles.
The SM has been succesful in explaining experimental phenomena but there is one particle not found yet, the Higgs boson, responsible for giving various particles their mass.

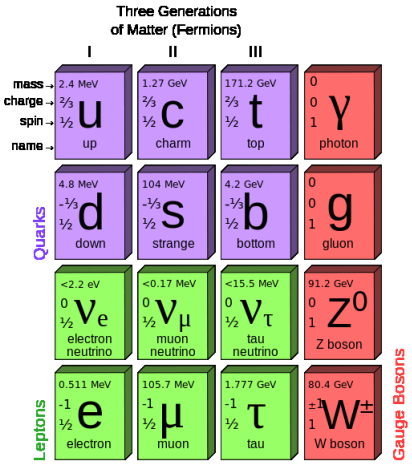

Figure 3: Standard Model of Particles

Hadronic matter can be further sub-divided into baryons and mesons. Baryons contain groups of three bound quarks (such as the proton and neutron) or antiquarks (such as the antiproton and antineutron), mesons contain bound quark-antiquark pairs. In both cases the quarks (and antiquarks) are confined by gluons. Under normal conditions it is not possible to observe free quarks, antiquarks and gluons. However, under extreme conditions of temperature or pressure, for example those similar to what is believed to have existed up until $10 - 5$ seconds after the Universe began, hadronic matter undergoes a phase transition into a hot dense soup of matter known as a Quark-Gluon Plasma (QGP) in which quarks, antiquarks and gluons become deconfined. [3]

1.5 K mesons

The family of strange particles includes all the particles which contain one or more strange quark or anti-quark. These includes the baryons and mesons.

In December 1947, Rochester and Butler published the cloud chamber photograph. Cosmic rays enter from the upper left and strike a lead plate producing a neutral particle, whose presence is revealed when it decays into two charged secondaries, π^+ and π^-. This led to the discovery of a neutral particle with atleast twice the mass of pion, it was called Kaon (K^0). The kaons behave like heavy mesons in some respect so they were included in meson family.

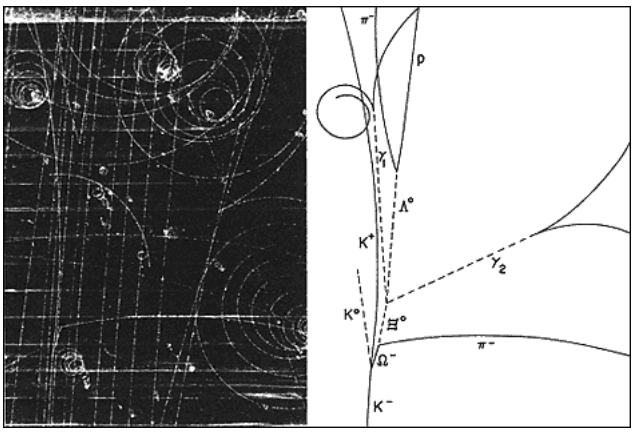

Figure 4: Cloud chamber photograph showing strange particle production

The physical neutral kaons are K^0 short (K_S^0) and K^0 long (K_L^0), denomination that comes from their life times. K_S^0 and K_L^0 are both quantum states given by linear combinations of K^0 ($d\bar{s}$) and $\bar{K}^0$ ($\bar{d}s$) assuming CPT invariance.

$$K^0 \longrightarrow \pi^+ + \pi^- \tag{1}$$

In 1950 another neutral particle was found by Anderson's group at Caltech. This time the products were a p^+ and a π^-. This particle was called Lambda ($\Lambda = uds$) and evidently it is higher than proton. It was placed in the Baryon's family.

$$\Lambda \longrightarrow p^+ + \pi^- \tag{2}$$

These Kaons and Lambda were called strange particles. They are produced copiously but they decay relatively slowly. The strange particles have the property of being produced in the strong interactions but their decay is due to the weak interaction. This property led to the introduction of a new quantum number, called strangeness, that is conserved in strong but not in weak interactions. The $K's$

carry strangeness $S = +1$ and Λ has $S = -1$. So, strangeness is conserved when these particles are produced and it is not conserved when these particles decay. So we never produce just one strange particle.

Some of the properties of K^0_S Λ and $\bar{\Lambda}$ are listed out in table 1

Table 1: Main characteristics of K^0_S , Λ^0 and $\bar{\Lambda}^0$.

Particles	Mass(MeV/c^2)	$c\tau(cm)$	charged decay	branching ratio (%)
K^0_S	497.61	2.68	$K^0_S \to \pi^+ + \pi^-$	69.2
Λ^0 and $\bar{\Lambda}^0$	1115.68	7.89	$\Lambda^0 \to p\pi^-, \bar{\Lambda}^0 \to \bar{p}\pi^+$	63.9

1.6 Analysis tools (ROOT and AliROOT)

AliRoot is the offline framework for the ALICE experiment. Its aim is to perform the reconstruction and analysis of physics data coming from simulated and real interactions. AliRoot makes use of ROOT framework, which is an object oriented framework based on C++. ROOT have several useful features for data processing, it includes C/C++ and command line interpreters, allows Parallel Processing (PROOF), has a graphical user interface and many statistical analysis tools (multidimensional histograms, fitting, random number generators, etc). AliRoot makes use of all ROOT facilities, and includes the geometry of ALICE detector. For data analysis in our project `ROOT::v5-28-00` and `AliRoot: :v4-21-27-AN` were used.

2 Analysis Work

2.1 Datasets

The selected data have been produced by the ALICE experiment on July 2010 from pp collisions at $\sqrt{s} = 7TeV$. The run number 126424 and 126425 are used from period LHC10d. 8 proton bunches interacted at the ALICE point and a minimum bias trigger configuration of detectors was imposed. As comparison there was also used the corresponding simulated data with PYTHIA event generator. Physics selection is applied to all the events which removes the unwanted events before any other selection criteria is applied.

2.2 V^0 track reconstruction and particles identification

K^0_S and Λ measurements are based on the reconstruction of secondary vertex V^0. V^0 particles are long-lived neutral particles which are reconstructed by their decay

to charged particles. In the reconstruction stage it is necessary to trace charged tracks and the V^0 back to within the target to the place where the proton beams interacted. This interaction point is known as the primary vertex. Reconstruction of V^0 decays requires finding oppositely charged tracks which are detached from the primary vertex and form a good vertex with an appropriate invariant mass.

The first stage of reconstruction begins by identifying possible V^0 candidates from raw data. Each positive track is compared to each negative track and, to be accepted as a possible V^0 candidate, the distance of closest approach of the two tracks must be less than a maximum limit, in this case $0.5cm$. Also tracks must have sufficiently large impact parameter with respect to the primary vertex, to be considered as secondary track. Once V^0 candidates are identified, we keep only those ones inside a given fiducial volume, from radius 1 to $100cm$ from the primary vertex. They are further sub-divided into K^0, Λ and $\bar{\Lambda}$ candidates, whose detectable decay modes are given in table 1. V^0 finding procedure also checks whether particle momentum associated with the V^0 candidate points back to the primary vertex. This is achieved by applying a cut on on the cosine of the angle ($\cos\theta_p > 0.99$)

When a V^0 particle decays in a magnetic field the two oppositely charged tracks which result will decay in one of two topologies: known as sailor orcowboy. Two tracks which bend away from one another are known as a sailor topology, two tracks which bend towards one another are known as a cowboy topology.The K^0S candidate must have two decay tracks with a cowboy topology. Additional selection criteria is applied based on particular decay topology to remove unwanted background. A clean event generated is shown in figure 5 which shows decay of K^0_S to $\pi^+\pi^-$ (cowboy topology) and Λ^0 decay to $p^+\pi^-$ (sailor topology).

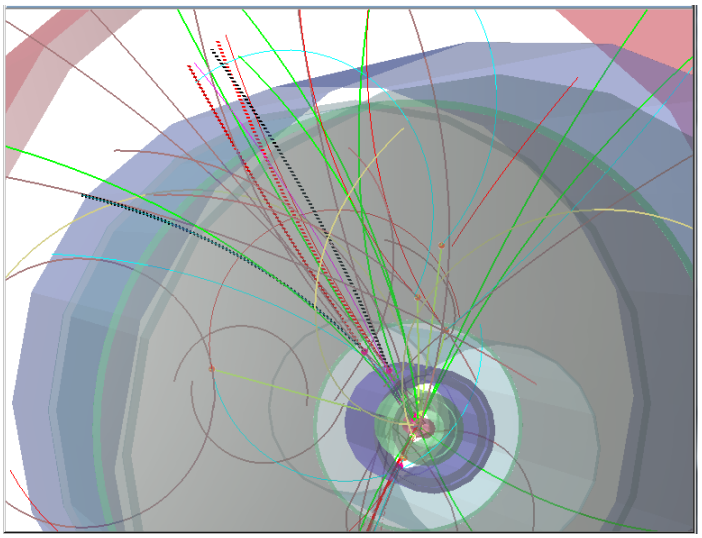

Figure 5: Event display showing sailor and cowboy topologies (alien:///alice/data/2010/LHC10d/000126425/ESDs/pass2/10000126425024.10 event 541)

Making use of Podolanski-Armenteros ellipses, we can ditinguish between

different hadrons. This is a two-dimensional plot which plots q_T against α. q_T is defined as the transverse component of either of the V^0 decay particles relative to the direction of the V^0(as by conservation of momentum both are the same) and α is defined as:

$$\alpha = \frac{q_L^+ - q_L^-}{q_L^+ + q_L^-} \tag{3}$$

where q_L^+ and q_L^- are the longitudinal momentum components of the positive and negative decay tracks respectively relative to the direction of the V^0. α measures the momentum asymmetry in the decay. The obtained distribution as shown in figure 6 shows that decay products of the $K_S^0, \pi^+\pi^-$ have the same mass and therefore their momenta are distributed symmetrically on average, while for decay of Λ the proton (antiproton) takes on average a larger part of the momentum and as a result the distribution is asymmetric. Thus three particles can be separated by making appropriate alpha selections.

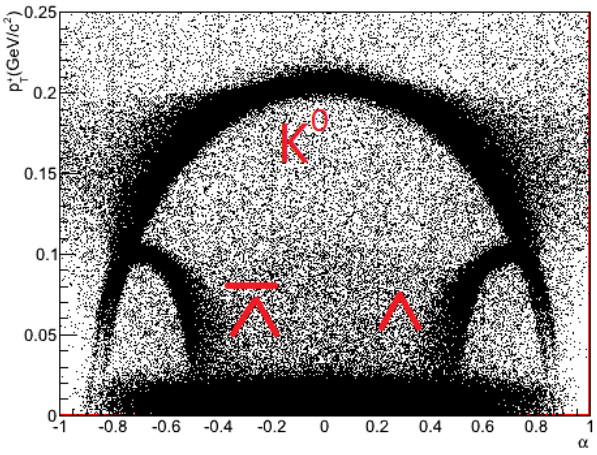

Figure 6: Podolanski-Armenteros ellipse

Additionally, we calculate the invariant mass of K_S^0, Λ and $\bar{\Lambda}$. Table 2 summarizes all the cuts applied for the identification of particles.

The real and simulated data mass distribution of K_S^0 candidates are shown in figure 7. Both distributions are comparable and yields match each other.

After applying all the cuts on real data distribution, we see the background is almost removed and figure 8 shows us the peak at the value of invariant mass of K_S^0.

The peak is fitted with a double gaussian and linear background as shown in figure 9. The value of mass comes out to be $0.4975 GeV/c^2$. This value can be compared to the PDG value described in table 1.

Parameter	Cut
Impact parameter of daughter tracks to the primary vertex (cm)	< 0.1
DCA between daughter tracks (cm)	< 0.05
L_{xyz} (cm)	> 1 < 100
Cosine of V^0 pointing angle	< 0.990
For K^0_S	
p_T^+ (GeV/c)	> 0.125
For Λ	
p_T^+ (GeV/c)	> 0.02 < 0.125
α	> 0.45
V^0 mass under K^0_S hypothesis (GeV/c^2)	< 0.47 > 0.53
For $\bar{\Lambda}$	
p_T^+ (GeV/c)	> 0.02 < 0.125
α	< -0.45
V^0 mass under K^0_S hypothesis (GeV/c^2)	< 0.47 > 0.53

Table 2: Cuts applied on different parameters for identification of K^0_S, Λ and $\bar{\Lambda}$.

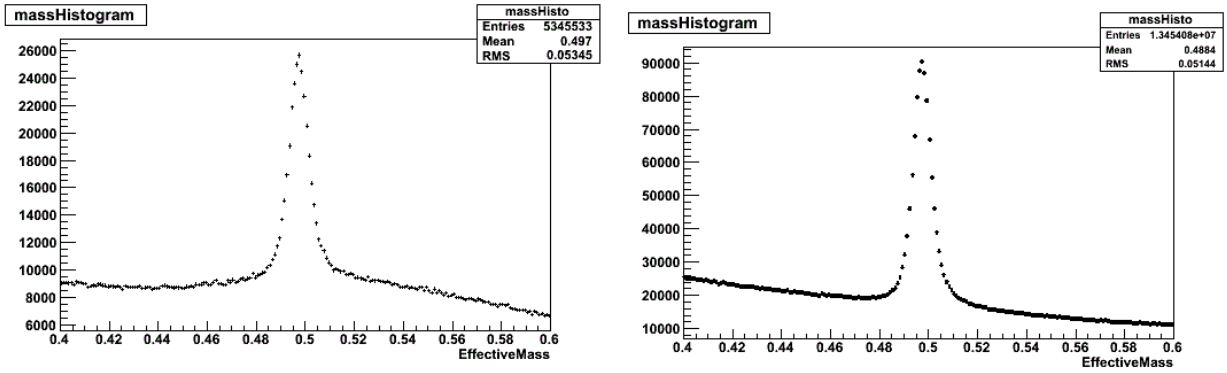

Figure 7: Invariant mass distribution (GeV/c^2)as given by, a. Real dataset. b. Simulated MC dataset

2.3 K^0 lifetime

The proper time measurement strategy is to construct the transverse decay length L_{xyz} of K^0. Transverse component is the component of decay length in the plane

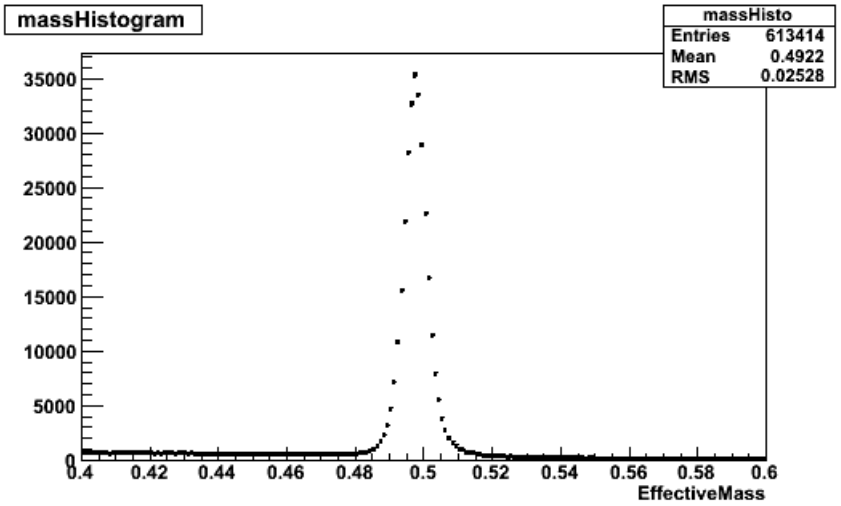

Figure 8: Invariant mass distribution (GeV/c^2)

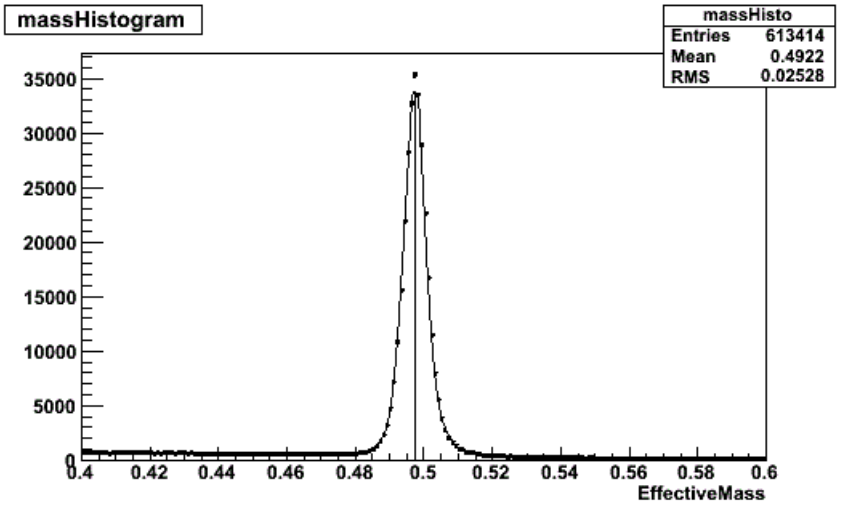

Figure 9: fitted peak giving the K0-mass value

perpendicular to the beam axis. A mass window from 0.48GeV to 0.52GeV around the peak is chosen and decay length distribution L_{xyz} of K_S^0 for both Real and Simulated data is obtained as shown in figure 10.

The proper time will be calculated using $c\tau$ distribution.

$$c\tau = \frac{L_{xyz}}{\beta\gamma} \tag{4}$$

We know that relativistic momentum is given by, $p = \gamma\beta m_0$ so, the above relation becomes:

$$c\tau = \frac{L_{xyz}}{p_T} m_{K^0} \tag{5}$$

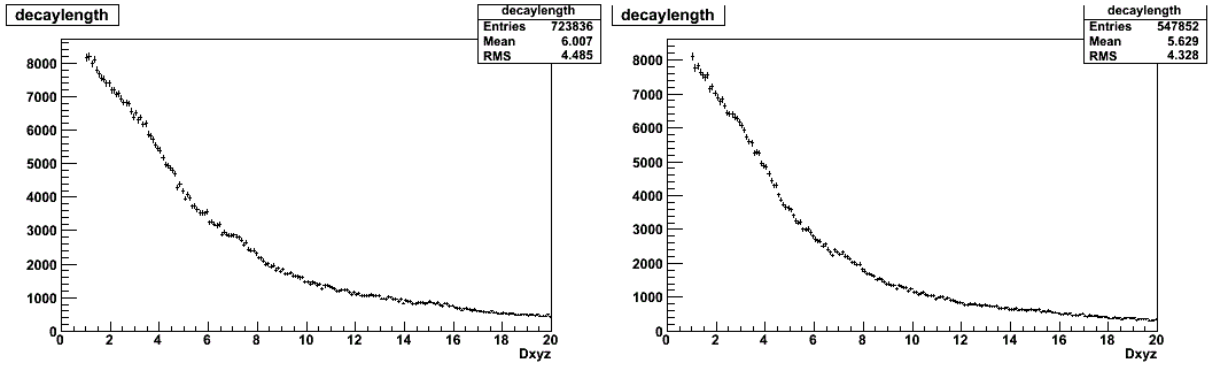

Figure 10: Decay length (cm) a. Real Data and b. Simulated Data

The $c\tau$ distribution follows an exponential distribution $\exp -\frac{L}{c\tau}$ and K^0 life time is the time constant of this distribution. The value of the mass of K^0 is used from PDG value. The plots are shown in figure 11.

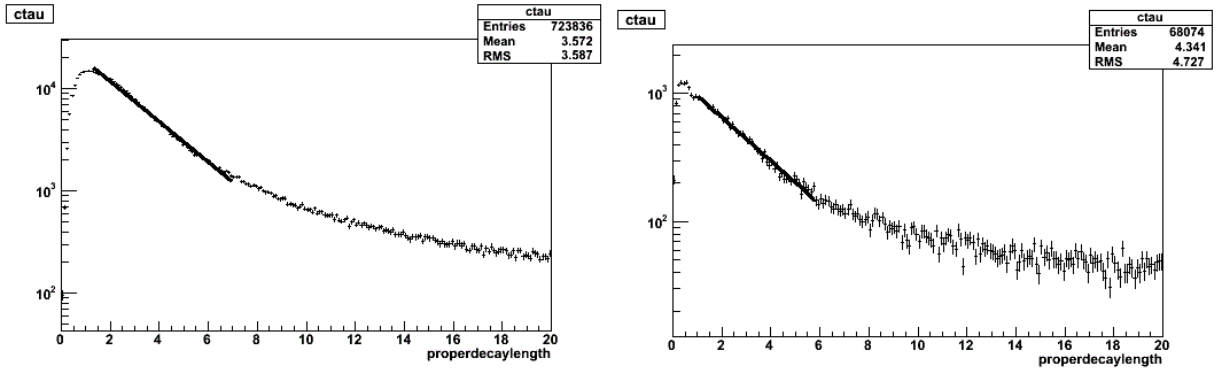

Figure 11: The $c\tau(cm)$ distribution for both Real and simulated Data a. Real Data and b. Simulated Data

Results are found for both distributions. For real data, $Slope = \frac{1}{c\tau} = 0.3988$ which gives us $c\tau = 2.507cm$. Thus life time of K^0 is determined to be $83.5ps$and for simulated data, slope is found out to be 0.3808 which gives us the value of $c\tau = 2.565$ and lifetime $t = 85.5ps$ compatible with the PDG values.

2.4 Multiplicity Dependence of K^0_s

The multiplicity dependence particles give us important information about characteristics of species. Figure 12a shows no. of K^0s changing with respect to no.of events selected from the mass window described earlier and 12b shows total multiplicity. Figure 13 is obtained by dividing previous two histograms and it gives us the multiplicity dependence of K^0.

As apparent, the trend is linear in the start showing increase in multiplicity

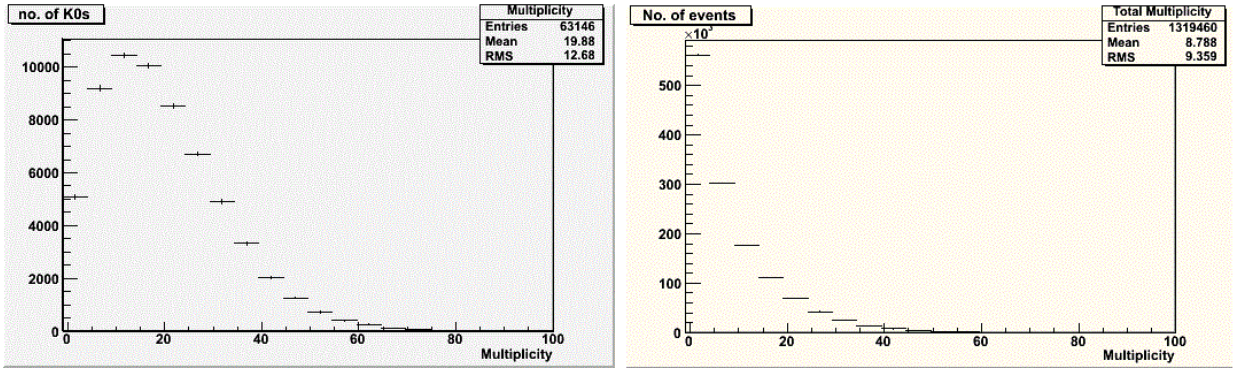

Figure 12: a. No. of events contributing to K^0 and b. Total no. of Events

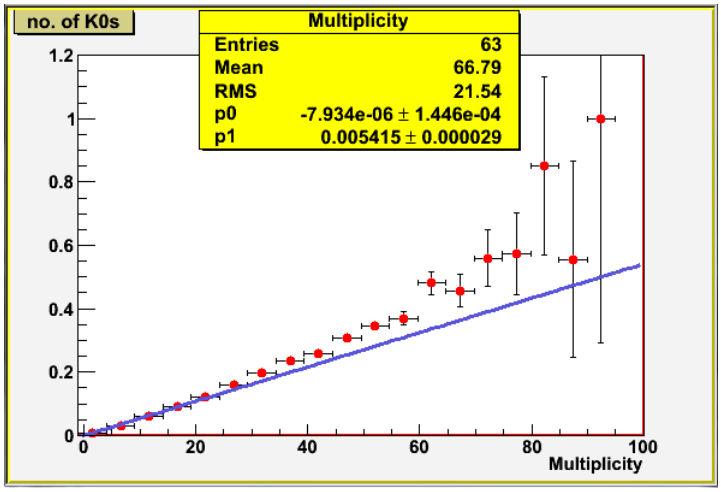

Figure 13: Multiplicity Dependence of K^0

as number of events increase. There is some deviation which means K^0 production happens faster than production of charged particles. Here, it is to be kept in mind though that K^0 yields are not corrected for background and efficiency which could change slightly with multiplicity. In addition, average p_t increases with multiplicity affecting efficiency differently for different charged particles and K^0s.

3 Conclusion

The results of studying reconstructed tracks from the data recorded by ALICE at $\sqrt{s} = 7TeV$ are presented in above sections. As we see, the basic kinematic properties of the tracks have been compared with the expectations from simulations. The multiplicity dependence of K^0_s is shown. Clear mass peak in the decay of K^0_s is reconstructed and its life time is determined. Both values of mass and lifetime are in agreement with PDG value.

4 Further discussion

The analysis can further be continued on different aspects like correcting data sets using results from Monte Carlo Simulation, determining errors and calculating uncertainties in experimental values which were not taken into account due to time constraints. The selection cuts for both K^0 and Λ particles were explained in previous sections so a similar analysis can be done for Λ and $\bar{\Lambda}$ particles to obtain kinematic information about these particles. Further, same analysis can be repeated for heavy ion (Pb-Pb) collisions and results can be compared with those obtained as a result of elementary ion (p-p) collisions.

5 Appendix

5.1 Invariant mass

Let's suppose we have a particle with energy E, rest mass m_0 and momentum p which decays in two particles with energies E_1 and E_2, rest masses m_{0_1} and m_{0_2} and momenta p_1 and p_2 respectively, so we have:

$$E = E_1 + E_2 \tag{6}$$

$$\vec{p} = \vec{p_1} + \vec{p_2} \tag{7}$$

Squaring equation 6:

$$E^2 = E_1^2 + E_2^2 + 2E_1E_2 \tag{8}$$

and substitute E^2 in 8 using the energy-momentum relation,

$$E^2 = m_0^2c^4 + p^2c^2 \tag{9}$$

we have:

$$m_0^2c^4 + p^2c^2 = m_{0_1}^2c^4 + p_1^2c^2 + m_{0_2}^2c^4 + p_2^2c^2 + 2E_1E_2 \tag{10}$$

or:

$$m_0^2c^2 = m_{0_1}^2c^2 + m_{0_2}^2c^2 - p^2 + p_1^2 + p_2^2 + \frac{2E_1E_2}{c^2} \tag{11}$$

substituting p^2 from equation (12) in 11

$$p^2 = p_1^2 + p_2^2 + 2p_1p_2\cos\theta \tag{12}$$

we get the invariant mass of particles 1 and 2, decay's product of the particle with rest mass m_0.

$$m_0^2c^2 = m_{0_1}^2c^2 + m_{0_2}^2c^2 + 2\left(\frac{E_1E_2}{c^2} - p_1p_2\cos\theta\right) \tag{13}$$

where m_0 is the particle's invariant mass. It follows that m_0 is also invariant under longitudinal boosts.

5.2 Rapidity and PseudoRapidity

Pseudorapidity is a spacial variable which describes the angle of a particle relative to the beam axis. It is denoted by η and is defined as:

$$\eta = -\ln(\tan\theta/2) \tag{14}$$

where θ is the angle between particle momentum $\vec{p}$ and the beam axis.
While rapidity is defined as follows:

$$y = \frac{1}{2}\ln\frac{E+p_z}{E-p_z} \tag{15}$$

where p_z is the longitudinal momentum or the component of momentum along the beam axis.

where p_z is the longitudinal momentum or the component of momentum along the beam axis and E is the total energy. Rapidity is a useful quantity as its shape is unaffected by a longitudinal Lorentz boost: i.e. the shape of the rapidity distribution is the same in whatever frame of reference, just shifted. For example, to go from the center of mass, cm, frame where the y distribution is centered on zero, to the frame measured in the laboratory, lab (used in fixed target experiments) is simply achieved by a shift in rapidity, described as below:

$$y_{lab} = y_{cm} + y_0 \tag{16}$$

where y_0 is a constant.
The rapidity of a particle is a measure of where in the collision it has come from. A rapidity of zero (in the cm system) implies the particle has come from the center of the collision. A positive or negative value of y implies the particle has come from the forward or backward region of the collision

We will show here as mass of the particle approaches zero, rapidity becomes equal to pseudorapidity.
We know that p_z is the longitudinal momentum along $z-axis$ defined as:

$$p_z = |\vec{p}|\cos\theta \tag{17}$$

putting the value of p_z above, we get,

$$y = \frac{1}{2}\ln\frac{E+|\vec{p}|\cos\theta}{E-|\vec{p}|\cos\theta} \tag{18}$$

Since momentum and energy are connected by this simple relation:

$$m^2 = E^2 - \vec{p}^{\,2} \tag{19}$$

substituing $|\vec{p}|$ from 19 in equation 18:

$$y = \frac{1}{2}\ln\frac{E+E\sqrt{1-\frac{m^2}{E^2}}\cos\theta}{E-E\sqrt{1-\frac{m^2}{E^2}}\cos\theta} \quad \Rightarrow \quad y = \frac{1}{2}\ln\frac{1+\sqrt{1-\frac{m^2}{E^2}}\cos\theta}{1-\sqrt{1-\frac{m^2}{E^2}}\cos\theta} \tag{20}$$

In the limit when mass goes to zero, $m \to 0$, we can simplify the relation as:

$$y = \frac{1}{2} \ln \frac{1 + \cos\theta}{1 - \cos\theta} \tag{21}$$

Using trigonometric identities and simplification, we can write $\cos\theta$ in terms of $\tan\theta$ as follows: since by half angle identities,

$$\sin^2\theta/2 = \frac{1 - \cos\theta}{2} \qquad \text{and} \qquad \cos^2\theta/2 = \frac{1 + \cos\theta}{2}$$

we can write $\tan^2\theta/2$ as:

$$\tan^2\theta/2 = \frac{\sin^2\theta/2}{\cos^2\theta/2} = \frac{1 - \cos\theta}{1 + cos\theta} \tag{22}$$

substituting in equation 21 we get,

$$y = \frac{1}{2} \ln \left[\left(\tan^2\theta/2 \right)^{-1} \right] \tag{23}$$

which gives us:

$$y = -\ln\left(\tan\theta/2\right) \tag{24}$$

Hence, in the limit when mass approaches zero, rapidity becomes equal to pseudo-rapidity.

5.3 Fixed Target and Colliding System Energy

Consider the collision of two particles, with rest masses m_1 and m_2 respectively; and energies E_1 and E_2 and momenta $\vec{p}_1$ and $\vec{p}_2$ in the laboratory system (LS). Their 4-momenta are:

$$p_{\mu_1} = (E_1, \vec{p}_1) \qquad \text{and} \qquad p_{\mu_2} = (E_2, \vec{p}_2) \tag{25}$$

and, in the center of mass system (CMS):

$$p'_{\mu_1} = (E'_1, \vec{p}\,'_1) \qquad \text{and} \qquad p'_{\mu_2} = (E'_2, \vec{p}\,'_2) \tag{26}$$

By the invariance of the scalar products, we have:

$$(p_{\mu_1} + p_{\mu_2})^2 = (p'_{\mu_1} + p'_{\mu_2})^2 \tag{27}$$

for the total 4-momentum of the collision.

In the CMS:

$$(p'_{\mu_1} + p'_{\mu_2})^2 = (E'_1 + E'_2)^2 - (\vec{p}\,'_1 + \vec{p}\,'_2)^2 \tag{28}$$

but as their momenta are equal and opposite:

$$(p'_{\mu_1} + p'_{\mu_2})^2 = (E'_1 + E'_2)^2 = E^2_{CMS} = s \tag{29}$$

in the LS,

$$(p_{\mu_1} + p_{\mu_2})^2 = m_1^2 + m_2^2 + 2(E_1E_2 + \vec{p}_1\vec{p}_2) \tag{30}$$

so, we have for the total energy in the CMS, the following relation:

$$s = m_1^2 + m_2^2 + 2(E_1E_2 + \vec{p}_1\vec{p}_2) \tag{31}$$

For a head-on collision with $m_1, m_2 << E_1, E_2$, we have:

$$s \simeq 4E_1E_2 \tag{32}$$

in a collider system with equal energies, the center of mass energy $\sqrt{s}$ rises linearly with E.
Consider now a fixed target collision where we have a particle (1) and another particle (2) comes and hit it. Since first particle is at rest, $\vec{p}_1 = 0$, and $E_1 = m_1$, then equation 31 becomes:

$$\begin{aligned} s &= m_1^2 + m_2^2 + 2m_1E_2 \\ s &\simeq 2m_1E_2 \end{aligned} \tag{33}$$

for a fixed-target collision the center of mass energy $\sqrt{s}$ rises as the square root of the incident energy.

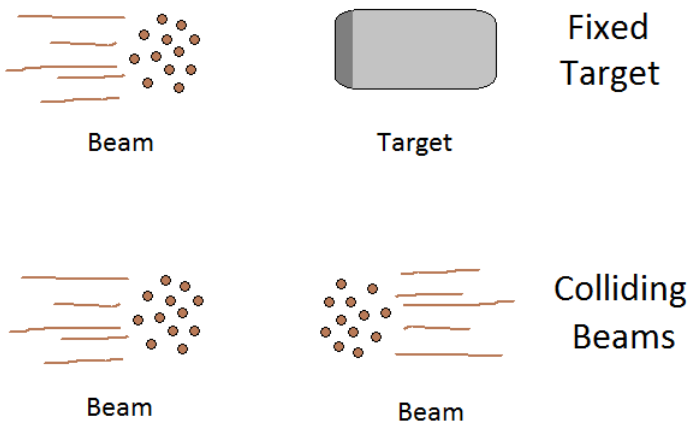

Figure 14: Fixed Target and Colliding beams

For collisions involving colliding beams, energy of center of mass is much higher than collisions involving fixed targets. Thus, experiments with colliding beams are preferred when we want to have high energy collisions.

References

[1] http://aliweb.cern.ch/

[2] http://aliceinfo.cern.ch/Public/Welcome.html

[3] http://etheses.bham.ac.uk/233/1/Bull05PhD.pdf

[4] http://www.star.bnl.gov/ gorbunov/main/node45.html

[5] K^0_S and Λ production in pp interactions at $\sqrt{s} = 0.9TeV$ and $7TeV$ measured with the ATLAS detector at the LHC (November 8, 2011)

[6] Strange particle production in proton-proton collisions at $\sqrt{s} = 0.9TeV$ with ALICE at the LHC (The ALICE collaboration)

[7] Track Reconstruction in CMS tracker, W. Adam, B. Mangano, T.Speer

[8] Introduction to Elementary Particles by David Jeffry Griffiths.